Volume 21, No 3 | International Journal of Radiation Research, July 2023

# Value of volume-rendering computed tomography for diagnosing different solitary pulmonary nodules and invasion depth in lung adenocarcinoma

**Y. Li[1#], J. Liu[2#], J. Zhou[3], L. Zhang[4*], X. Li[4*]**

[1]*Department of Respiratory, Ruijin Hospital, Luwan Branch, Shanghai Jiaotong University School of Medicine, Shanghai 200025, China*
[2]*Department of Medicine, Minhang Hospital, Fudan University, Shanghai 201199, China*
[3]*Department of Anesthesiology, Ruijin Hospital Luwan Branch, Shanghai Jiaotong University School of Medicine, Shanghai 200025, China*
[4]*Department of Critical Care Medicine, Minhang Hospital, Fudan University, Shanghai 201199, China*

► ***Original article***

***Corresponding author:***
*Xiang Li, M.D. and Lu Zhang, B.M.*
***E-mail:*** *XXang_L123@126.com*

**Received:** December 2021
**Final revised:** April 2022
**Accepted:** July 2022

***Int. J. Radiat. Res., July 2023; 21(3): 369-375***

**DOI:** 10.52547/ijrr.21.3.3

***Keywords:*** *Breast cancer, radiotherapy, lymphocytes, chromosomal aberration, bioindicator.*

#these authors contributed equally to this work.

## ABSTRACT

***Background*:** We aimed to analyze the value of volume rendering (VR) in diagnosing different solitary pulmonary nodules (SPNs) with diameter less than 1.0 cm and assessing invasion depth in lung adenocarcinoma. ***Materials and Methods*:** In total, 908 patients with SPN that was confirmed by postoperative pathology were included, followed by an analysis of the imaging characteristics (including microvascular sign, vascular convergence, lobulation, and spiculation) of malignant and benign SPN based on VR. Moreover, the detection rates of imaging signs of three types of malignant SPNs (pure ground grass nodule, pGGN; part-solid nodule; and solid nodule) classified by SPN density and three invasion depths of adenocarcinoma (pre-invasion lesion, PIL; micro invasive adenocarcinoma, MIA; and invasive adenocarcinoma, IAC) were also analyzed. ***Results*:** The microvascular sign detection rate was higher while vascular convergence and spiculation detection rates were lower in malignant SPN than in benign SPN. The microvascular sign possessed high sensitivity (82%) and specificity (72%) in predicting malignant and benign SPNs. The microvascular sign detection rate decreased while vascular convergence, lobulation, and spiculation detection increased with the rising density of malignant SPN. Furthermore, the detection rates of the four imaging signs all increased with the adenocarcinoma invasion depth. Microvascular sign showed good detecting ability in low density SPNs pGGN (81.8%), part-solid nodules (95.8%), and in all three invasion depths of adenocarcinoma (PIL [68.2%], MIS [95.3%], and IAC [87.2%]). ***Conclusion*:** These imaging features distinguished by VR exhibited an excellent differential diagnostic ability of various SPNs as well as invasion depth of lung adenocarcinoma.

## INTRODUCTION

Primary bronchogenic cancer is the leading cause of cancer death from malignant tumors worldwide [1]. Solitary pulmonary nodules (SPNs) are solitary, round-like, dense shadows with a maximum diameter of less than 3.0 cm in the lung parenchyma that is completely surrounded by pulmonary parenchyma and without other pulmonary abnormalities [2-4]. With the popularization of computed tomography (CT) of the chest, the detection rate of SPNs is increasing yearly [5]. The imaging features of SPNs are common manifestations of various benign and malignant diseases, and there are no special symptoms and signs in clinical practice. Increasing studies have revealed that the diagnosis of SPN has a great impact on the clinical treatment [6-8]. Therefore, the accurate diagnosis of SPNs is very important. However, it is a challenge for imaging technology to differentially diagnose malignant from benign SPNs [9, 10]. Lack of reliable early diagnosis techniques of malignant SPN has plagued clinicians and radiologists, and exploration of specific imaging signs of malignant SPN for clinical application has aroused sustained and extensive attention of researchers.

Volume rendering (VR) is one of the most commonly used post-processing techniques for CT images [11]. According to the CT value and surface characteristics of each voxel, VR assigns a different color and transparency in the imaging volume. Through the reconstruction of the CT image and the simulation of a light source, a three-dimensional image of the tissue structure is presented [12]. VR images have the characteristics of high spatial resolution and can visually reproduce the surface characteristics of SPN and its relationship with surrounding tissues in three-dimensional space. Although a growing body of studies have sought the

[ Downloaded from ijrr.com on 2026-11-22 ]

[ DOI: 10.61186/ijrr.21.3.369 ]

qualitative diagnosis of SPN by investigating the relationship between SPN and blood vessels [13-16], the qualitative diagnosis of SPN with a diameter less than 1.0 cm still challenges clinicians due to its insignificant imaging features. CT is widely used to identify the invasion depth of lung adenocarcinoma, while fewer publications report on identifying the depth of adenocarcinoma via the VR imaging sign. Kim et al. found that tumor size was significantly correlated with the depth of adenocarcinoma invasion [17]. The correlation of specific imaging characteristics and the invasion depth of adenocarcinoma tend to be ambiguous.

Previous studies mainly focused on CT diagnosis of SPNs with diameter less than 3 cm, while this study mainly focused on SPNs with diameter less than 1 cm. This retrospective study collected data from patients with SPN by postoperative pathology. We aimed to analyze the imaging signs like microvascular sign, vascular convergence, lobulation, and spiculation of SPN, using VR technology to investigate the relationship between SPNs and blood vessels as well as the invasion depth of adenocarcinoma. The study highlights the role of VR technology in the diagnosis of SPN and invasion depth of lung adenocarcinoma, which will facilitate a better understanding of the value of VR in the diagnosis of SPN and adenocarcinoma invasion.

## MATERIALS AND METHODS

### *Patients*

This retrospective study was approved by the Ruijin Hospital Luwan Branch Ethics Committee, Shanghai JiaoTong University School of Medicine (No. LWEC201603) and all cases between January 1, 2014, to December 31, 2018, were collected from the respiratory department. In total, data from 908 patients were collected. All participants provided written informed consent.

According to the size of SPN set by the experimental goal and excluding the influence of treatment, antibiotics were given when SPN is first discovered, so as to avoid the inclusion of inflammatory nodules. The inclusion criteria of patients in our study were as follows: (1) patients with a single pulmonary nodule with a diameter ≤ 1 cm that was detected by chest CT and (2) patients with suspected non-small cell lung cancer who underwent surgery at the same time. The exclusion criteria were as follows: (1) patients with a history of cancer; (2) patients receiving anti-tumor therapy, such as radiotherapy, chemotherapy, or targeted therapy, adrenocortical hormone, or other non-steroidal anti-inflammatory drugs; (3) patients with recent pulmonary infection; and (4) patients with multiple pulmonary nodules. The end points were as follows: (1) two years after the expiration of observation; (2) patient death; (3) the case was diagnosed as a malignant tumor; or (4) lost to follow up.

The postoperative pathology of all cases was in line with the 2011 International Association for the Study of Lung Cancer (IASLC) and American Thoracic Society multidisciplinary classification standard of lung adenocarcinoma jointly published by the American Thoracic Society (ATS) and European Respiratory Society (ERS) [18]: (1) atypical adenomatous hyperplasia (AAH): mild to moderate atypical hyperplasia of focal epithelial cells, without interstitial inflammatory reaction and fibrous hyperplasia; (2) carcinoma in situ (AIS): the diameter of the lesion is ≤ 3.0 cm, and the malignant tumor cells grow along the alveolar wall, without interstitial, vascular, or pleural infiltration; (3) micro invasive adenocarcinoma (MIA): the diameter of the lesion is ≤ 3.0 cm, with infiltration, but the infiltration range is ≤ 0.5 cm; (4) invasive adenocarcinoma (IAC): the diameter of the lesion is ≤ 3.0 cm and the infiltration range is > 0.5 cm.

### *CT scanning and image analyzing*

For CT scanning, patients were trained to breathe in and hold their breath. Then, all lung fields from the entrance of the pleura to the level of bilateral adrenal glands were scanned using a SIEMENS 64-slice spiral CT (SOMATOM Definition AS). The scanning thickness and spacing was set as 5 mm. Thin-slice scanning was performed in the area where SPN was located. The thickness and spacing of the slices were 1 mm. The CT image data were then transmitted to the GE ADW 4.3 post-processing workstation (General Electric Healthcare, Milwaukee, WI, USA), and VR was performed. Two senior radiologists, with over 20 years of experience in chest CT, independently classified the SPNs into three types based on the density of the solid components of the SPNs [19]: (1) pure ground grass nodule (pGGN): hazy increased attenuation in the lung that does not obliterate the bronchial and vascular margins; (2) solid nodule: homogenous soft-tissue attenuation; (3) part-solid nodule: consists of both pGGN and solid soft-tissue attenuation [20, 21]. Based on VR, the imaging signs of SPNs, including microvascular sign, vascular convergence sign, lobulation, and spiculation, were then analyzed by an experienced chest radiologist in a blinded manner, who was blinded to the study-group assignments.

Microvascular signs are mainly manifested by the microvasculature entering the SPN and connecting with the microvasculature of the nodule. Vascular convergence sign refers to the vessels converging to a nodule that are not adjoined to or contacting the edge of the nodule. Lobulation manifests as an uneven and curved edge of an SPN. The main manifestation of spiculation is the extension of the SPN to the surrounding tissues and the adjacent lung parenchyma.

[ Downloaded from ijrr.com on 2026-11-22 ]

[ DOI: 10.61186/ijrr.21.3.369 ]

### *Statistical analysis*

The statistical software SPSS 18.0 (SPSS, Inc., Chicago, IL, USA) was used for statistical analysis. The obtained data were expressed as the mean ± standard deviation (SD) or as percentage (for invariable parameters). Sensitivity, specificity, positive predictive value and negative predictive value of VR were analyzed with receiver operator characteristic curve (ROC) curve analysis. Correlation analysis was performed using the chi-square ($\chi^2$) test and trend $\chi^2$ test. A value of $P < 0.05$ was considered significant.

## RESULTS

### *General clinical data*

All 908 patients with SPNs were confirmed by postoperative pathology, including 315 males (34.7%) and 593 females (65.3%), and the size of nodules was 0.73±0.31 cm. The imaging signs of SPN were analyzed by VR, including microvascular sign, vascular convergence, lobulation, and spiculation (figure 1). According to postoperative pathological detection, 825 cases (90.9%) were ultimately diagnosed as the malignant SPN group and the remaining 83 (9.1%) cases were determined as the benign SPN group. Detailed results from the pathological diagnosis were shown in table 1. The average age of 908 patients was 56.15±10.85, of which 149 aged less than 45 years old, 414 were 46 ~ 60 years old, and 345 cases were over 60 years old. A total 93% of patients (148 cases) were under 45 years old, 86.2% patients (357 cases) were 46 ~ 60 years old, and 38.8% (134 cases) were over 60 years old.

**Table 1.** The pathological diagnosis results of benign and malignant SPN cases.

| | Pathology | Cases | Percentage |
|---|---|---|---|
| **Malignant SPN group** | | 825 | |
| | Squamous cell carcinoma | 1 | 0.1% |
| | Adenomatous atypical hyperplasia (AAH) | 37 | 4.5% |
| | Adenocarcinoma in situ (AIS) | 290 | 35.3% |
| | Microinvasive adenocarcinoma (MIA) | 279 | 33.8% |
| | Invasive adenocarcinoma (IAC) | 218 | 26.3% |
| **Benign SPN group** | | 83 | |
| | Fibrous hyperplasia | 48 | 6.0% |
| | Hamartoma | 13 | 15.7% |
| | Tuberculous granuloma | 8 | 9.6% |
| | Fungal granuloma | 6 | 7.2% |
| | Lymph gland | 8 | 9.6% |

SPN, Solitary pulmonary nodule.

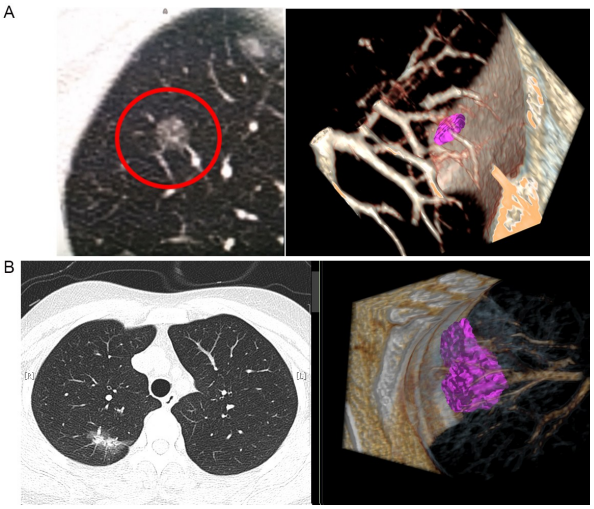



**Figure 1. (A)** Axial computed tomography (CT) images show pure nonsolid nodule of the right lower lobe with microvascular sign in the pure ground grass opacity. Micro invasive adenocarcinoma was found on pathologic examination. **(B)** Axial CT images show a pure nonsolid nodule of the right lower lobe, with microvascular sign in the part-solid nodules, and vascular convergence sign surround the nodules. Invasive adenocarcinoma was found on pathologic examination.

### *Comparison of imaging signs between malignant and benign SPN groups*

The microvascular sign detection rate was significantly higher while that of vascular convergence and spiculation was significantly lower in the malignant SPN group than in the benign SPN group ($P < 0.001$). There was no significant difference in the detection rate of lobulation between benign and malignant SPN groups ($P > 0.050$) (table 2). In addition, the sensitivity, specificity, and positive predictive value of tumor microvascular CT imaging in predicting malignant SPN were 82.4%, 72.3%, and 96.7%, respectively, which were significantly higher than other imaging signs (table 2), demonstrating that the microvascular sign performed well in identifying the malignant SPN from benign SPN. Furthermore, the ROC analysis showed that the area under the curve (AUC) value of the microvascular sign was 0.773, further demonstrating its effective predicting value.

### *Comparison of imaging signs of three types of malignant SPN*

According to the different SPN densities, 825 cases of malignant SPN were classified into three types: pGGN in 632 (76.6%) cases, part-solid nodules in 144 (17.5) cases, and solid nodules in 49 (5.9%) cases. In different types of malignant SPN, significant differences were observed in the detection rates of microvascular sign, vascular convergence, lobulation, and spiculation (table 3, $P<0.001$). With the increase of SPN density, the detection rate of microvascular sign was decreased significantly (trend $P<0.001$), while the detection rates of vascular convergence

[ Downloaded from ijrr.com on 2026-11-22 ]
[ DOI: 10.61186/ijrr.21.3.369 ]

sign, lobulation, and spiculation were increased remarkably (trend $P$<0.001) (table 3). Notably, the microvascular sign showed higher detection rates in pGGN (81.8%) and part-solid nodule (95.8%), demonstrating that the microvascular sign was appropriate for diagnosing pGGN and part-solid nodules. Vascular convergence and spiculation also possessed considerable ability in the diagnosis of solid nodules, with detection rates of 69.4% and 79.6%, respectively. Microvascular sign and lobulation were inadequate in the diagnosis of solid nodules, with 49.0% detection rates for both.

### *Comparison of SPN imaging features of adenocarcinoma with different depth of invasion*

Among 825 cases of malignant SPN, 824 were adenocarcinoma and 1 was squamous cell carcinoma. According to the depth of invasion of adenocarcinoma, 824 adenocarcinomas were divided into the pre-invasion lesion (PIL) group (including AAH and AIS) with 327 cases (39.7%), MIA group with 279 cases (33.8%), and IAC group with 218 cases (26.5%). Compared with the imaging signs among the three groups, there were significant differences in the detection rates of tumor microvascular sign, vascular convergence, lobulation, and spiculation in SPN with different depth of invasion ($P$<0.001). As the depth of invasion of adenocarcinoma increased, the detection rates of tumor microvascular sign, vascular convergence, lobulation, and spiculation increased (trend $P$<0.001) (table 4). Notably, the detection rates of microvascular sign for PIL (68.2%), MIA (95.3%), and ICA (87.2%) groups were all high, while the detection rates of vascular convergence, lobulation, and spiculation were less so. The detection rates of vascular convergence, lobulation, and speculation for IAC were higher than PIL and MIA, contributing 30.3%, 40.0% and 41.7% in the IAC groups respectively. These outcomes also highlight the pivotal role of tumor microvascular sign for diagnosing the tumor invasion depth.

**Table 2.** Comparison of imaging signs between malignant and benign SPN groups.

| Imaging features | Malignant SPN [n (%)](n=825) | Benign SPN [n (%)] (n=83) | $\chi^2$ | P | Sensitivity (%) | Specificity (%) | PPV (%) | NPV (%) |
|---|---|---|---|---|---|---|---|---|
| Microvascular sign | 679 (82.3) | 23 (27.7) | 128.14 | < 0.001 | 82.4 (95% CI: 9.7 ~ 84.9) | 72.3 (95% CI: 62.7 ~ 81.9) | 96.7 | 9.1 |
| Vascular convergence | 93 (11.3) | 24 (28.9) | 20.91 | < 0.001 | 11.3 (95% CI: 9.1 ~ 13.4) | 71.1 (95% CI: 61.3 ~ 80.8) | 79.5 | 7.5 |
| Lobulation | 122 (14.8) | 19 (22.9) | 3.78 | > 0.05 | 14.8 (95% CI: 12.4 ~ 17.2) | 77.1 (95% CI: 68.1 ~ 86.1) | 86.5 | 8.3 |
| Spiculation | 149 (18.1) | 30 (36.1) | 15.58 | < 0.001 | 18.1 (95% CI: 15.4 ~ 20.7) | 63.9 (95% CI: 53.5 ~ 74.2) | 83.2 | 7.3 |

SPN, Solitary pulmonary nodule. PPV: Positive predictive value; NPV: Negative predictive value.

**Table 3.** Imaging signs of three types of malignant SPN.

| Imaging features | pGGN (n = 632), n (%) | Part-solid nodules (n = 144), n (%) | Solid nodules (n = 49), n (%) | $\chi^2$ | *P* | Trend $\chi^2$ | *P* |
|---|---|---|---|---|---|---|---|
| Microvascular sign | 517 (81.8) | 138 (95.8) | 24 (49.0) | 55.57 | < 0.001 | 4.42 | < 0.05 |
| Vascular convergence | 15 (2.4) | 44 (30.6) | 34 (69.4) | 269.03 | < 0.001 | 266.43 | < 0.001 |
| Lobulation | 57 (9.0) | 41 (28.5) | 24 (49.0) | 83.55 | < 0.001 | 83.43 | < 0.001 |
| Spiculation | 53 (8.4) | 57 (39.6) | 39 (79.6) | 210.41 | < 0.001 | 209.10 | < 0.001 |

SPN, Solitary pulmonary nodule; pGGN: pure ground grass nodule.

**Table 4.** Comparison of SPN imaging features of adenocarcinoma with different depth of invasion [n (%)].

| Imaging features | PIL (n=327) | MIA (n=279) | IAC (n=218) | $\chi^2$ | *P* | Trend $\chi^2$ | Trend *P* |
|---|---|---|---|---|---|---|---|
| Microvascular sign | 223 (68.2) | 266 (95.3) | 190 (87.2) | 82.23 | < 0.001 | 42.72 | < 0.001 |
| Vascular convergence | 10 (3.1) | 17 (6.1) | 66 (30.3) | 108.37 | < 0.001 | 87.93 | < 0.001 |
| Lobulation | 10 (3.1) | 25 (9.0) | 87 (40.0) | 152.56 | < 0.001 | 129.76 | < 0.001 |
| Spiculation | 16 (4.9) | 42 (15.1) | 91 (41.7) | 122.84 | < 0.001 | 114.32 | < 0.001 |

SPN, Solitary pulmonary nodule; PIL, pre-invasion lesion; MIA, micro invasive adenocarcinoma; IAC, invasive adenocarcinoma.

## DISCUSSION

As public health awareness and the popularity of CT examination have increased, more and more SPN cases have been diagnosed. CT imaging has the advantages of speed, high-contrast resolution, and little influence of respiratory movement and organ peristalsis on images. It can effectively observe micro-vessels, especially in lung tissue with high air content, and is considered the first choice for follow-up SPN observation. However, there is considerable overlap in the features of malignant and benign SPNs that may cause an erroneous diagnosis of pulmonary nodules [22]. Malignant and benign SPNs lack specificity in traditional two-dimensional images, so it is difficult to observe the fine morphological features of SPNs. VR can reconstruct the two-dimensional images to show the spatial relationship of SPNs and their surrounding blood vessels in three-dimensional space. All of the SPN cases in this study were reconstructed by VR on the basis of thin-slice CT. The morphology of the SPNs and their relationships with peripheral blood vessels were observed.

In the early stage of tumor development, vasculature remodeling or neoangiogenesis is a common initiating event. Microvascular sign are mainly manifested by thin-slice CT scanning of the

[ Downloaded from ijrr.com on 2026-11-22 ]

[ DOI: 10.61186/ijrr.21.3.369 ]

point at which the microvasculature enters the SPN and connects with the microvasculature of the nodule [23]. New tumor blood vessels in the SPN not only indicate an increased blood supply, but also represent a change in the tumor's biological behavior, from inert dormancy to malignant invasive development. Wang et al. found that compared to the non-lung cancer group, patients in the lung cancer group had a higher number of vessels attached to a nodule [23]. Furthermore, some microvascular characterizations, such as blood flow and yielding blood volume are found useful in distinguishing malignant from benign lung nodules [24]. In this study, we found that the detection rate of microvascular sign in malignant SPN group (82.3%) was significantly higher than in the benign SPN group (27.7%). With the increase of SPN density in the malignant SPN group, the detection rate of microvascular sign was significantly decreased. Normally, solid nodules are less dangerous than GGN. Other studies also revealed that SPN combined with vessel relationship or microvascular sign might strongly suggest malignancy [16, 23, 25], which is similar to our results. Furthermore, the sensitivity, specificity and positive predictive value of tumor microvascular sign in predicting malignant SPN were comparatively high. The ROC analysis suggested that the AUC was 0.773, further indicating an effective predicting value of microvascular sign. Therefore, we speculate that microvascular sign may play an important role in the qualitative diagnosis of malignant and benign SPNs less than 1.0 cm in diameter as well as different densities of malignant SPNs.

Vascular convergence sign refers to the vessels converging to a nodule that are not adjoined to or contacting the edge of the nodule, and is mainly observed in peripheral subsolid lung cancers [26]. It is reported that vascular convergence sign is expressed in subsolid nodules with a malignancy rate of 85.2%, while expressing much lower in 40.0% of benign nodules [27]. In another study, no significant difference in the detection rate of vascular convergence sign was identified between benign (17.31%) and malignant nodules (17.07%) [28]]. Wei *et al*. [29] reported similar results in their study, that no significant difference in benign (4.52%) and malignant (5.56%) SPNs was exhibited. These results were inconsistent with our results that the detection rate of vascular convergence was significantly higher for the benign than for the malignant SPN group, but this may be due to the small benign sample size in our study. Moreover, the vascular convergence in malignant focal ground-glass opacity (fGGOs) is revealed to be significantly higherthan that in benign fGGOs [30]. This result is consistent with our results that the detection rate of vascular convergence increased with higher SPN density in the malignant SPN group, reflecting a reliable result.

The main manifestation of the lobulation is that the edge of SPN is uneven and curved. Pathological analysis shows that this is caused by the asynchronous differentiation and growth of tumor cells at the edge of an SPN and the fibrous hyperplasia and contraction of the nodule [31]. It is reported that deep lobulation in the malignant SPN lesions has a great diagnostic value [4]. Wang *et al*. demonstrated that lobulation of SPN could be intuitively displayed by three-dimensional CT reconstruction, which might contribute to distinguishing the benign and malignant cases [28]. The detection rate of lobulation in benign and malignant nodules were 19.51% and 63.46%, respectively, which indicating a higher detection rate of lobulation in malignant nodules. In another two studies, a similar result was also found, that the incidence of lobulation of malignant SPN was higher than that of benign SPN cases [29, 32]. While in our study, the differences in detection rate of lobulation between malignant and benign SPN groups were not significant, which disagreed with previous research [28, 29, 32]. Furthermore, the detection rate of lobulation in malignant SPN was only 14.8, which might be due to small nodule diameter (less than 1.0 cm). Furthermore, the detection rate showed a gradually increasing trend with the malignant SPN density.

The main manifestation of spiculation is a result of the extension of SPN to the surrounding tissues and the adjacent lung parenchyma. The pathological basis of spiculation is caused by interlobular septal thickening and fibrosis caused by obstruction of pulmonary vessels or lymphatic channels filled with SPN cells [26]. Spiculation is an important shape feature for measurement of the malignancy of SPN and had a high diagnostic value for malignant SPN [29, 33, 34]. In different studies, the detection rate of spiculation varies largely. Yang *et al*. suggested that the detection rates of spiculation for benign and malignant SPN are 13.7% and 32.3%, respectively [35]. Wang *et al.* found that the detection of spiculation in benign and malignant SPN are 17.07% 59.62%, respectively [28]. Wei *et al*. also suggested a similar result that the detection rate of spiculation in benign and malignant SPN was 25.16% and 67.9%, respectively [29]. Although the detection rate varied in different studies, these results all demonstrate that the detection rate of speculation in malignant SPNs is higher than in benign ones. While in our results, the relationship of detection rate of benign and malignant SPNs were reversed (36.1% and 18.1%, respectively). Inversely, we found a higher detection in the benign SPN group (36.1%) and the detection rate of spiculation gradually increased with increasing density of malignant SPN. Collectively, although we cannot confirm the diagnostic value of vascular convergence sign, lobulation, and spiculations in identification of benign and malignant SPNs, they may be valuable in the qualitative

[ Downloaded from ijrr.com on 2026-11-22 ]

[ DOI: 10.61186/ijrr.21.3.369 ]

diagnosis of solid nodules of malignant SPN.

The detection rate of tumor microvascular sign, vascular convergence, lobulation and spiculation were different in the three different invasion depths of adenocarcinoma in our study, which further suggested that the imaging feature played a vital role in the identification of malignant tumors. Yue et al. found a significant difference in the detection rate of microvascular sign between the MIC and IAC groups, which was inconsistent with our results [16]. They also emphasized the diagnostic value of vascular convergence in lung adenocarcinoma. The detection rate of microvascular sign in MIC and IAC groups were relatively high, reaching 71.43% and 41.98%, respectively. Gao et al. found that the detection rate of lobulation and spiculation between PIL and MIA exhibited no significant differences [25]. Although the detection rate in various studies is not similar, the diagnostic role of microvascular sign, vascular convergence, lobulation, and spiculation in different invasion depth of lung adenocarcinoma should be emphasized. The incidence of microvascular sign in PIL, MIA, and IAC are all high and higher depth of invasion led to a higher detection rate, which means the presence of microvascular sign indicates an increased risk of lung adenocarcinoma. Similarly, incidence of vascular convergence, lobulation, and spiculation are also valuable indicators of lung adenocarcinoma.

The study has several advantages. First, VR can present SPN panoramas more vividly and stereoscopically and reveal SPN surface features more intuitively through multi-angle and multi-plane rotation. Second, we diagnosed SPN with a diameter less than 1.0 cm, which was less common in previous studies. Third, we highlight the potential significance of microvascular sign in diagnosing SPN and adenocarcinoma invasion.

Nevertheless, there are several limitations in this study. First, the experimental results may be more inclined to pGGN due to the different sample sizes of the three types of SPN. Second, the sample size of benign SPN was small, which may also cause statistical deviation and is also the reason why analysis of the imaging features among different densities of benign SPNs has been omitted. Future investigations with large sample sizes of SPN cases, especially part-solid and solid nodes, are still required to further explore the association between malignant SPN and blood vessels. The relationship between SPNs and blood vessels revealed by VR is of great significance to the early diagnosis of malignant SPNs. With the rising detection rate of SPNs, effectively identifying malignant SPNs will benefit patients. We believe that the relationship between SPNs and blood vessels should play an important role in the differential diagnosis of SPNs and is worthy of further study and verification.

## CONCLUSION

Through multi-angle and multi-plane rotation, VR presents the SPN landscape more vividly and stereoscopically, revealing SPN surface features more intuitively. Based on VR technology, our data revealed different imaging features in SPNs less than 1.0 cm in diameter. The diagnostic ability of imaging features including microvascular sign, vascular convergence, lobulation, and spiculation were consistent in identifying the different SPNs and the invasion depth of adenocarcinoma. The relationship between SPN and blood vessels revealed by VR was of great significance to the differential diagnosis of benign and malignant SPN and is worthy of further study and verification.

***Conflict of interests*:** The authors declare that they have no conflict of interests.

**Funding:** This work was supported by Qualitative Diagnosis of Small Pulmonary Nodule Based on the Chest CT Three-dimensional Reformation (No. 164411973400) and The role of AI recognition combined with serum FR+CTC abundance in accurate diagnosis of pulmonary nodules(No. HLM202104).

***Authors' contributions*:** J.Z. carried out the conception and design of the research, Y.L. participated in the Acquisition of data. Yong Li carried out the Analysis and interpretation of data. J.L. and L.Z. participated in the design of the study and performed the statistical analysis. Y.L. and X.L. conceived of the study, and participated in its design and coordination and helped to draft the manuscript and revision of manuscript for important intellectual content. All authors read and approved the final manuscript.

## REFERENCES

1. Smith RA, Andrews KS, Brooks D, *et al.* (2017) Cancer screening in the United States, 2017: a review of current American Cancer Society guidelines and current issues in cancer screening. CA: *A Cancer Journal for Clinicians, **67**(2): 100-121*.
2. Wyker A and Henderson WW (2021) Solitary pulmonary nodule, in StatPearls. 2021, StatPearls Publishing: Treasure Island (FL).
3. Bai C Choi C-M, Chu CM, *et al.* (2016) Evaluation of pulmonary nodules: clinical practice consensus guidelines for Asia. *Chest, **150**(4): 877-893*.
4. Wahidi MM, Govert JA, Goudar RK, *et al.* (2007) Evidence for the treatment of patients with pulmonary nodules: when is it lung cancer?: ACCP evidence-based clinical practice guidelines. *Chest, **132**(3): 94S-107S*.
5. Ettinger DS, Aisner DL, Wood DE, *et al.* (2018) *NCCN Guidelines Insights: Non-Small Cell Lung Cancer, Version 5.2018. J Natl Compr Canc Netw, **16**(7): 807-821*.
6. Prakashini K, Babu S, Rajgopal K, Kokila KR (2016) Role of computer aided diagnosis (CAD) in the detection of pulmonary nodules on 64 row multi detector computed tomography. *Lung India: official organ of Indian Chest Society, **33**(4): 391*.
7. Lin J-z, Zhang L, Zhang C-y, Yang L, *et al.* (2016) Application of gemstone spectral computed tomography imaging in the characterization of solitary pulmonary nodules: Preliminary result. *Journal of Computer Assisted Tomography, **40**(6): 907-911*.

[ Downloaded from ijrr.com on 2026-11-22 ]

[ DOI: 10.61186/ijrr.21.3.369 ]

8. Calheiros JLL, de Amorim LBV, de Lima LL, *et al.* (2021) *T*he Effects of Perinodular Features on Solid Lung Nodule Classification. *J Digit Imaging,* ***34****(4): 798-810*.
9. Truong MT, Sabloff BS, Ko JP (2010) Multidetector CT of solitary pulmonary nodules. *Thoracic Surgery Clinics,* ***20****(1): 9-23*.
10. Shi Z, Wang Y, He X (2016) Differential diagnosis of solitary pulmonary nodules with dual-source spiral computed tomography. *Experimental and therapeutic medicine,* ***12****(3): 1750-1754*.
11. Bankier AA, MacMahon H, Goo JM, *et al.* (2017) Recommendations for measuring pulmonary nodules at CT: a statement from the Fleischner Society. *Radiology,* ***285****(2): 584-600*.
12. Naeem MQ, Darira J, Ahmed MS, *et al.* (2021) Comparison of maximum intensity projection and volume rendering in detecting pulmonary nodules on multidetector computed tomography. *Cureus,* ***13****(3): p. e14025*.
13. Han F, Wang H, Zhang G, *et al.* (2015) Texture feature analysis for computer-aided diagnosis on pulmonary nodules. *Journal of Digital Imaging,* ***28****(1): 99-115*.
14. Dhara AK, Mukhopadhyay S, Saha P, *et al.* (2016) Differential geometry-based techniques for characterization of boundary roughness of pulmonary nodules in CT images. *Int J Computer Assisted Radiology and Surgery,* ***11(3):*** *337-349.*
15. Buty M, Xu Z, Gao M, *et al.* (2016). Characterization of lung nodule malignancy using hybrid shape and appearance features. in International Conference on Medical Image Computing and Computer-Assisted Intervention. 2016. Springer.
16. Yue X, Liu S, Yang G, Z, *et al.* (2018) HRCT morphological characteristics distinguishing minimally invasive pulmonary adenocarcinoma from invasive pulmonary adenocarcinoma appearing as subsolid nodules with a diameter of ≤ 3 cm. *Clinical Radiology,* ***73****(4): 411. e7-411. e15*.
17. Kim KH, Ryu S-Y, Lee HY, *et al.* (2019) *Evaluating the tumor biology of lung adenocarcinoma: A multimodal analysis. Medicine,* ***98****(29)*.
18. Travis WD, Brambilla E, Noguchi M, *et al.* (2011) International Association for the Study of Lung Cancer/American Thoracic Society/European Respiratory Society:International multidisciplinary classification of lung adenocarcinoma: executive summary. *Proc Am Thorac Soc,* ***8****(5): 381-5*.
19. Daković-Bjelaković M, Popović J, Antić M, (2017) Analysis of the anatomical variations of the supraorbital transcranial passage in Southeast Serbian population on volume rendered CT scans. *Acta medica Medianae,* ***56****(3): 81-87*.
20. Cruickshank A, Stieler G, Ameer F (2019) Evaluation of the solitary pulmonary nodule. *Intern Med J,* ***49****(3): 306-315*.
21. Hansell DM, Bankier AA, MacMahon H, *et al.* (2008) Fleischner Society: glossary of terms for thoracic imaging. *Radiology,* ***246****(3): 697-722*.
22. Wu L, Cao G, Zhao L, *et al.* (2018) Spectral CT analysis of solitary pulmonary nodules for differentiating malignancy from benignancy: the value of iodine concentration spatial distribution difference. *BioMed research international,* ***2018,*** *https://www.hindawi.com/journals/bmri/2018/4830659/***.**
23. Wang X, Leader JK, Wang R, *et al.* (2017) Vasculature surrounding a nodule: A novel lung cancer biomarker. *Lung Cancer,* ***114****: 38-43*.
24. Sitartchouk I, Roberts HC, Pereira AM, *et al.* (2008) Computed tomography perfusion using first pass methods for lung nodule characterization. *Investigative Radiology,* ***43****(6): 349-358*.
25. Gao F, Sun Y, Zhang G, *et al.* (2019) *CT characterization of different pathological types of subcentimeter pulmonary ground-glass nodular lesions. The British Journal of Radiology,* ***92****(1094): 20180204*.
26. Snoeckx A, Reyntiens P, Desbuquoit D, *et al.* (2018) Evaluation of the solitary pulmonary nodule: size matters, but do not ignore the power of morphology. *Insights into Imaging,* ***9****(1): 73*.
27. Hu H, Wang Q, Tang H, *et al.* (2016) Multi-slice computed tomography characteristics of solitary pulmonary ground-glass nodules: Differences between malignant and benign. *Thoracic cancer,* ***7****(1): 80-87*.
28. Wang, X, Lv L, Zheng Q, *et al.* (2018) Differential diagnostic value of 64-slice spiral computed tomography in solitary pulmonary nodule. *Experimental and Therapeutic Medicine,* ***15****(6): 4703-4708*.
29. Wei Y, Bo Y, Liyun X, *et al.* (2016) Establishment of a clinical prediction model of solid solitary pulmonary nodules. *Chinese Journal of Lung Cancer,* ***19****(10)*: *705-710*
30. Fan L, Liu S, Li Q, *et al.* (2012) Multidetector CT features of pulmonary focal ground-glass opacity: differences between benign and malignant. *The British Journal of Radiology,* ***85****(1015): 897-904*.
31. Han G, Liu X, Soomro NQ, *et al.* (2017) *Empirical driven automatic detection of lobulation imaging signs in lung CT. BioMed Research International,* ***2017,*** *https://www.hindawi.com/journals/bmri/2017/3842659/.*
32. He Q, Fei Y, Ping D, *et al.* (2014) *Radiology, and T. affiliated, comparative study of MSCT and pathological findings of solitary pulmonary nodules. Chongqing Medicine,* ***43****(29):4.*
33. Dhara AK, Mukhopadhyay S, Alam N, Khandelwal N (2013) Measurement of spiculation index in 3D for solitary pulmonary nodules in volumetric lung CT images. in *Medical Imaging 2013: Computer -Aided Diagnosis*. 2013. I*nternational Society for Optics and Photonics.* ***8670,*** *DOI: 10.1117/12.2006970.*
34. Yang D, Li Y, Liu J, *et al.* (2010) Study on solitary pulmonary nodules: Correlation between diameter and clinical manifestation and pathological features. Zhongguo fei ai za zhi= *Chinese Journal of Lung Cancer,* ***13****(6): 607-611*.
35. Yang D, Li Y, Liu J, *et al.* (2010) Study on solitary pulmonary nodules: correlation between diameter and clinical manifestation and pathological features. *Zhongguo Fei Ai Za Zhi,* ***13****(6): 607-11*.


[ Downloaded from ijrr.com on 2026-11-22 ]

[ DOI: 10.61186/ijrr.21.3.369 ]

[ DOI: 10.61186/ijrr.21.3.369 ] [ Downloaded from ijrr.com on 2026-11-22 ]